IEEE Access
Multidisciplinary ⋮ Rapid Review ⋮ Open Access Journal

Received 31 May 2023, accepted 30 June 2023, date of publication 10 July 2023, date of current version 17 July 2023.

Digital Object Identifier 10.1109/ACCESS.2023.3293642

RESEARCH ARTICLE

Impact of Indoor Distributed Antenna System on RF-EMF Global Exposure

TAGHRID MAZLOUM, (Member, IEEE), SHANSHAN WANG, (Member, IEEE), AND JOE WIART, (Senior Member, IEEE)

Chaire C2M, Télécom Paris, Institut Polytechnique de Paris, 91120 Palaiseau, France

Corresponding author: Taghrid Mazloum (taghrid.mazloum@cea.fr)

This work was supported in part by the company TéléDiffusion de France (TDF group).

ABSTRACT The deployment of Distributed Antenna Systems (DAS) in poorly covered indoor areas has been a strategy to improve and extend radio-frequency (RF) coverage. However, this may imply a rise in the risk perception related to human exposure to electromagnetic fields (EMF), despite the existence of protection limits. Therefore, the objective of the current study is to analyze the overall impact of the installation of indoor DAS on the global human exposure. This analysis takes into account both downlink exposure, which includes exposure from outdoor base stations and indoor DAS, as well as uplink exposure induced by mobile phones. To this end, we carried out measurement campaigns in the premises of an organization and two subway stations in France, with the capability to selectively activate or deactivate the DAS antennas. The global exposure is evaluated using the 'Exposure Index (EI)' metric, which was developed as part of the European project LEXNET. The EI metric takes into consideration the exposure induced by both base stations and mobile devices, as well as the specific usage service (such as data or voice calls). The results have shown that deploying indoor DAS implies a reduction in the global EMF exposure while improving the quality of the cellular network connectivity. In addition to the impact of the usage service of mobile phones, the extent of EMF decrease is heavily influenced by the presence of additional RF sources. Specifically, significant reductions in EMF exposure have been observed in locations with minimal additional RF sources, whereas relatively lower reduction factors have been observed in locations with additional RF sources.

INDEX TERMS Distributed antenna system, radio-frequency electromagnetic field (RF-EMF), human exposure, exposure index, indoor coverage, measurements.

I. INTRODUCTION

With the increasing demand for wireless communications, seamless services have become essential regardless of the environment. Considering that human spends the majority of their time indoors (approximately 90% of the day [1]), research efforts have been dedicated to indoor propagation, coverage, and throughput [2]. In certain indoor environments, such as underground subway stations, shopping malls, and company premises, radio coverage can be extremely poor due to the positioning of antennas outside the premises. Moreover, with new environmental constraints linked to energy saving, buildings are designed to limit the environmental impact and reduce heat loss (a.k.a *Haute Qualité Environmentale*, HQE) [3], implying an attenuation of radio-frequency (RF) waves propagated through. Because of that, investigations have been conducted with new types of indoor base station antennas, such as a distributed antenna system (DAS), which is a network of spatially distributed antennas connected to a common source [4], [5], [6]. Deploying DAS in indoor environments has the potential to extend wireless coverage and improve service quality. With DAS, each antenna covers a relatively small localized area, ensuring closer proximity to users. However, this deployment raises concerns about the potential health risks associated with exposure to electromagnetic fields (EMF), despite the existence of

The associate editor coordinating the review of this manuscript and approving it for publication was Sandra Costanzo.

protection limits [7], [8]. Therefore, it is crucial to respect rules and guidelines for EMF exposure in order to ensure the safe deployment of any wireless communication network.

Human exposure encompasses both downlink (DL) and uplink (UL) exposure. DL exposure refers to EMF radiations emitted by distant sources such as base stations, femtocells, and DAS antennas. On the other hand, UL exposure is induced by nearby wireless devices, particularly mobile phones, regardless of whether they are held close to the human body or placed few centimeters away. UL exposure assessment is challenging due to the close proximity of user equipment (UE) to the human body. Furthermore, the UE output power is variable as it is adapted to network conditions through the transmit power control algorithm [9]. Consequently, it is important to note that DL and UL exposures usually exhibit correlated behaviors; when one increases, the other often decreases [10]. When the connection quality is very poor, the UE may radiate at the maximum power level allowed by the system. We note that people often underestimate the UL exposure, while they tend to overestimate the DL exposure, possibly due to the perception that base stations continuously emit at higher transmit power [11], [12].

In the literature, DL exposure has been extensively assessed through simulations and measurements, as reviewed in [13] for indoor scenarios. However, little works have focused on assessing UL exposure, especially in indoor environments. With the densification of cellular networks, especially the deployment of femtocells and small cells (resulting in a heterogeneous network), researchers have started studying the impact of this new network architecture on EMF exposure, taking into account both DL and UL. In this context, several in-situ measurements were carried out, considering indoor femtocells [14], [15], [16] and outdoor small cells [17], [18], [19], [20], and comparing them with macro cells. These studies covered various technologies, including the global system for mobile communication (GSM) for small cells deployed in trains [16], the universal mobile telecommunications system (UMTS) for indoor femtocells [14], [15], and both UMTS and long term evolution (LTE) for outdoor small cells [17], [18], [19], [20]. The measurements were carefully designed to cover a wide dynamic range of connection quality. Nonetheless, machine learning and artificial intelligence algorithms have been recently investigated to exploit the collected measured data and thereby predict and build an RF exposure map [21], [22], [23], [24]. Furthermore, researchers are actively addressing EMF exposure from newly deployed fifth-generation (5G) networks [25], [26], [27], [28], [29].

Different assessment strategies have been considered for DL and UL exposures. The mobile phone emitted power (TX), received power (RX) as well as data throughput have been recorded using drive test solutions (i.e., commercial software modified phones dedicated to record network parameters), e.g., Azenquos [30], QualiPoc Android from Rohde & Schwarz [31], and Nemo Handy from Keysight [32]. Moreover, in the context of epidemiological measurement campaigns, the characterization of individuals' daily life exposure is performed with non-commercial mobile phone applications such as XMobiSense [33] and a novel miniature personal exposimeter called Devin [34]. Devin is essentially a probe with additional electronics attached to the mobile phone cover [34]. When measuring DL exposure, the electric field (E-field) strength emitted by base station antennas has been measured using spectrum analyzer or personal exposimeter [14], [18], [20]. Alternatively, it has been monitored in a given area by deploying sensor networks [21], [35], [36]. A review on EMF measurement equipment can be found in [37] and [38].

When conducting compliance testing, DL and UL exposures need to be examined separately to ensure that regulatory limits are met. However, it is important to consider both sources together when evaluating global EMF exposure in real-world conditions, especially when assessing the impact of newly deployed technologies. Hence, we need to provide a comprehensive and accurate evaluation of the overall global exposure, which takes into account all of the RF sources that a person may be exposed to. In previous works such as [15] and [16], the total dose metric has been utilized. This metric calculates the product of the specific absorption rate (SAR) and the duration of exposure, providing an accumulated exposure over time. However, for evaluating average global exposure, the exposure index (EI) introduced in the European (EU) project LEXNET [11], [39], [40], [41] has been employed. EI takes into account the overall EMF exposure of a population within a specific area and duration, providing an average representation of exposure. More details about the EI are found in Section II.

After a comprehensive review of the literature, it has been observed that there is a significant research gap regarding the evaluation of the impact of indoor DAS on global EMF exposure. To address this need, an extensive measurement campaign was carried out in various environments, including the organization's premises (referred to as the campus) and two underground subway stations located in France. The campus served as a representative workplace environment where individuals spend the whole day. In contrast, the underground subway stations were selectively chosen as they are frequently crowded with people. The measurements covered a wide range of conditions and considered various usage services. These services included data uploading, voice over LTE (VoLTE), voice calls, and WhatsApp video calls, all operating across fourth-generation (4G) and third-generation (3G) frequency bands. By conducting measurements in these distinct settings and with the capability to activate or deactivate the DAS antennas, the study aims to provide comprehensive insights into the EMF exposure resulting from indoor DAS installations.

The paper is organized as follows. Section II introduces the concept of the global exposure EI. Section III describes

the measurement campaigns, including an overview on the indoor environments and a description of the protocols employed for both UL and DL measurements. Section IV presents the separate results of DL and UL, as well as their combination into EI. A general discussion is provided in Section V. Finally, we conclude the paper in Section VI.

II. GLOBAL EXPOSURE

Global exposure provides an accurate and comprehensive assessment of a person's overall exposure, including both DL and UL. It takes into account all potential sources of RF radiations that an individual may be exposed to, such as mobile phones, base stations, femtocells, and WiFi routers. In order to assess the global exposure induced simultaneously by all these sources, a novel exposure metric has been defined within the framework of the EU project LEXNET [11], [12], [39]. The EI metric covers the global EMF exposure of a population over a given time frame in a specific geographical area, incurred by a particular wireless telecommunication network or a set of networks. The way to build the EI is based on a chain of exposures covering all the relevant configurations we are dealing with, as depicted in Fig. 1. Individual exposure contributions are aggregated over different radio access technologies, cell types, usage services, etc. Further details about the formulation and the calculation of the EI are given in [11], [12], and [39], with some comprehensive examples on EI integration in [40] and [41].

In the present work, we consider a partial EI in order to emphasize the impact of deploying indoor DAS on the global exposure. Thus, we simplify the calculation of EI by considering few configurations of interest and ignoring all the other ones. The partial EI is averaged over a given exposure time duration (T) and integrates contributions from several technologies at different frequency bands (f) and from different usage services (u). Indeed, EI is calculated by weighting the measured incident power density ($\bar{S}_f^{inc}$) from each source by a DL reference SAR value (SAR_f^{DL}), and on the other hand, by weighting the mobile phone output power ($\bar{P}_{f,u}^{TX}$) for each usage service by a corresponding UL reference SAR value ($SAR_{f,u}^{UL}$). Both quantities provide the amount of RF energy absorbed by the body tissue. More clearly, the average partial EI is computed as:

$$EI = \frac{1}{T}\sum_f \left[t_f^{DL} \times SAR_f^{DL} \times \bar{S}_f^{inc} + \sum_u t_{f,u}^{UL} \times SAR_{f,u}^{UL} \times \bar{P}_{f,u}^{TX} \right], \quad (1)$$

where t_f^{DL} and $t_{f,u}^{UL}$ are the exposure time duration for DL and UL (per usage service u), respectively. We note that $\bar{S}_f^{inc}$ and $\bar{P}_{f,u}^{TX}$ are average values obtained from measurements, where the former is derived from the E-field strength values.

The individual exposure contributions rely on the SAR (expressed in W/Kg), which depends on several aspects, including the anatomy, the dielectric properties of human biological tissues, and the source itself (e.g., its emitted power, its relative location, and the frequency band). Within the LEXNET project, a set of numerical dosimetric simulations, e.g., Finite Difference in Time Domain and Finite Integration Technique, has been conducted to provide a comprehensive matrix of raw reference SAR values [12], [39], [42], [43]. These simulations have considered different numerical human models, postures (e.g., sitting and standing), service usages (e.g., voice and data), and frequency bands. The UL reference SAR ($SAR_{f,u}^{UL}$) has been calculated for various wireless devices (including smartphones, tablets, and laptops) and normalized to a transmitted power of 1 W. The DL reference SAR (SAR_f^{DL}) has been obtained using a plane wave model and normalized to a received power density of 1 W/m^2. These normalized SAR values can be whole-body (WBSAR) or localized SAR values. WBSAR values are obtained by averaging SAR over the whole body mass, while localized SAR values are assessed over specific organs, and for regulatory compliance, over a 10g cube. In Table 1, the reference WBSAR values are given for an adult model Duke (a male of 34 years old from the Virtual Family database [44]), while using a mobile phone in two different postures and at different frequency bands.

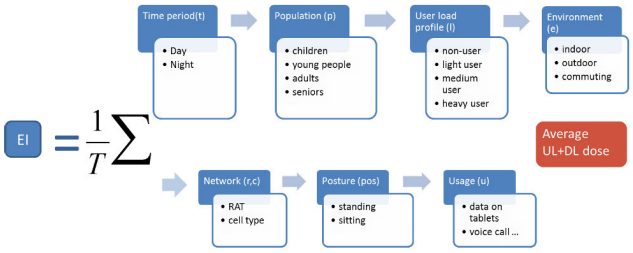

FIGURE 1. EI concept and formulation: the chain of exposure [12], [39].

TABLE 1. Reference whole-body SAR data for an adult model Duke while using a mobile phone [11].

WBSAR (W/Kg)		Frequency band		
		900 MHz	1940 MHz	2600 MHz
Voice Sitting	DL	0.0056	0.0043	0.0039
	UL	0.012	0.0052	0.0047
Voice Standing	DL	0.0052	0.0046	0.0042
	UL	0.012	0.0052	0.0053
Data Sitting	DL	0.0046	0.0043	0.0038
	UL	0.0056	0.0081	0.0037
Data Standing	DL	0.0052	0.0047	0.0042
	UL	0.0049	0.0039	0.0029

III. MEASUREMENT DESCRIPTION AND PROTOCOLS

A. MEASUREMENT ENVIRONMENTS

During almost two weeks on November 2021, measurement campaigns were carried out in an organization's building (referred to as the campus) and two underground subway stations located in France. These indoor locations have been deployed with DAS with the initial motivation being to

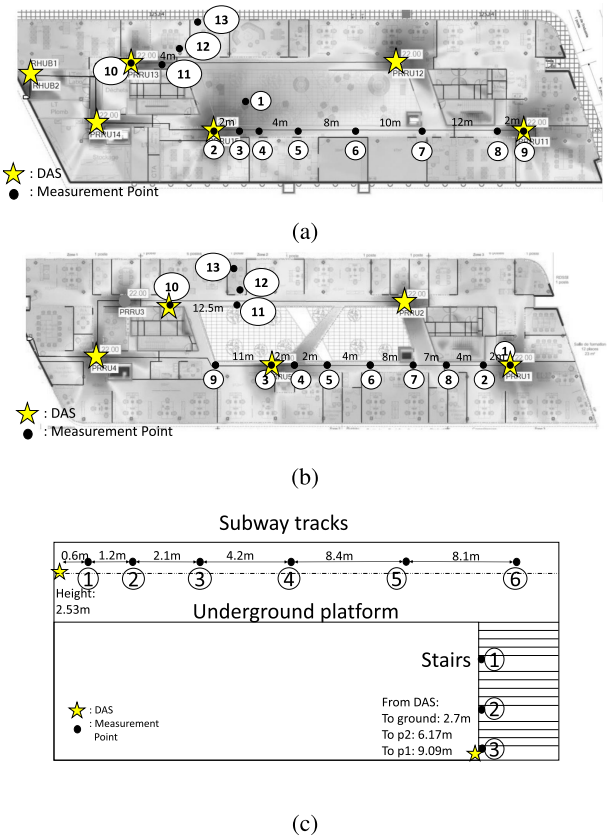

FIGURE 2. The distribution of measurement points and DAS antennas on (a) : the campus Fl1, (b): the campus Fl2, and (c): both SS1 underground platform and stairs.

provide good quality of service by extending the coverage of the outdoor cellular network. On the one hand, the campus has been built to limit energy leakage. Because of that, the signals coming from outdoor base station antennas do not guarantee good quality of service to users inside the building. Moreover, according to public accessible database (i.e., cartoradio [45]), the closest outdoor base station to the campus is located relatively far away, at a distance of about 610 m. Regarding the subway stations, multiple outdoor base stations are closely deployed around each station but they weakly pass through the underground floors and platforms. We refer to each subway station by Subway Station 1 (SS1) and Subway Station 2 (SS2).

The campus is a 4-floor building, where each floor has a ring-shaped layout and all the offices are distributed along the ring. The measurements were realized at two floors, i.e., floor 1 (Fl1) and floor 2 (Fl2), whose floorplans are shown in Fig. 2a and 2b. It is worth noting that several omni-directional ceiling-mounted DAS antennas are distributed throughout the same floor but also across different floors, all belonging to the same DAS system. Each DAS antenna is connected via optical fiber to a central unit known as the Master Unit, which provides the interface with the base station. This interface allows the Master Unit to receive wireless signals from the base station and efficiently distribute them to all the connected antennas within the DAS network. In this system, the DAS antennas operate over the 2600 MHz and 2100 MHz frequency bands for 4G and 3G wireless connections, respectively, serving a single operator.

Within SS1, measurements were performed on three different levels: the underground platform, the ground floor, and a very long staircase that connects underground and ground floors. While the ground floor is deployed with a ceiling-mounted omnidirectional DAS antenna, the other two are deployed with wall-mounted directive DAS antennas. Within SS2, we carried out measurements at the underground platform and the ground floor, where wall-mounted directive DAS antennas are installed. The DAS in both stations operates almost over all cellular bands (ranging from 700 MHz to 2600 MHz) of the four French operators. Similarly to the DAS system deployed on the campus, the DAS antennas in both subway stations, located at different floors and within the tunnels, are all part of the same DAS network. This arrangement is optimized to ensure that wireless signals are distributed evenly throughout the stations and tunnels, providing seamless wireless coverage for passengers in motion inside the train or in the subway station. It is important to note that, for security reasons, the directional DAS antennas within the tunnels were not switched off during all the measurements. This configuration may have an impact on the results if the RF signals emitted by these DAS antennas reach the underground platform, especially when the DAS antenna on the platform is switched off. Nonetheless, this setup represents a realistic use-case scenario where an additional far-away RF source is present.

For each considered environment, measurement points were selected to cover each floor according to several distances to the DAS antenna, thus covering a large dynamic range. Fig. 2 shows the distributions of these measurement points on each floor of the campus, SS1 platform and SS1 ground. SS2 platform shares nearly the same measurement points distributions as SS1 platform, shown in Fig. 2c. The locations of DAS antennas are marked with yellow stars.

B. DOWNLINK MEASUREMENT PROTOCOL

The DL exposure is assessed by measuring the electric field (E-field) strength using the Tektronix USB RSA306B, which is a real-time spectrum analyzer (RTSA). For EMF exposure measurement, the RTSA is modified to incorporate RF switching across the three axes of the tri-axial antenna. This modification allows for isotropic E-field strength measurements, which are calculated as the root sum square of the three components of the E-field (E_x, E_y, and E_z) obtained from the tri-axial antenna. The equipment setup is illustrated in Fig. 3.

Regarding the measurement design, we first identified, for each DAS antenna, the specific point where the E-field strength reaches its maximum value. This was accomplished by scanning the surrounding environment using a wideband field meter. Subsequently, in addition to that maximum point, we selected several other measurement points to ensure

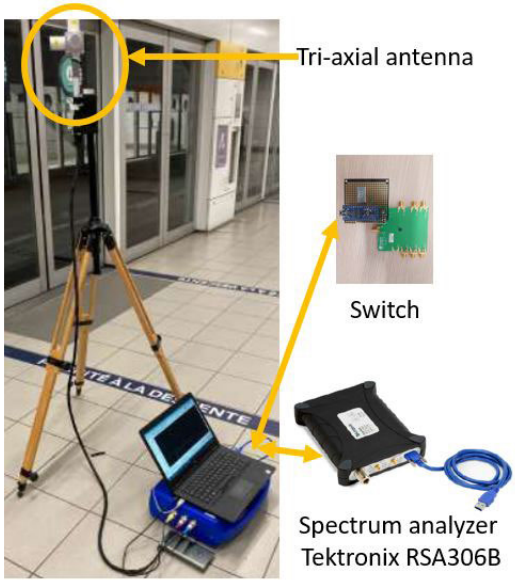

FIGURE 3. The real-time spectrum analyzer Tektronix RSA306B, connected to a tri-axial antenna via a switch.

coverage of all potential user locations on each floor. At each measurement point, the tri-axial antenna was placed at a height of 1.5 m and the measurement process consisted of 30 repetitions with a total duration of approximately 15 min. The E-field measurement was carried out across all the frequency bands of the DL for all network providers. This enables the computation of the total E-field by integrating the squared values over all the available frequency bands. The measurements were conducted twice, with the DAS antennas being alternately turned on and off. We refer to these scenarios as 'DAS on' and 'DAS off', respectively. We note that these measurements do not follow an accredited protocol such as that of the ANFR protocol [46], which concerns conformity control and aims to measure at 3 different heights at specifically the point where the wideband E-field strength is the highest.

C. UPLINK MEASUREMENT PROTOCOL

The UL exposure is characterized using a drive test solution (the Nemo Handy from KeySight [32], installed on Samsung Galaxy S8 and S20 5G). The drive test solution is a modified-software based mobile phone that allows recording network parameters. The UL exposure depends on multiple factors, including the power emitted by the phone and its relative position with respect to the user. These parameters are directly influenced by the phone usage. Additionally, for certain usages, the data throughput also plays a role as it is inversely proportional to the duration of UL exposure time. Considering the intermittent nature of the UL exposure, the Nemo Handy was scheduled to automatically perform the following usages: 1) Circuit voice call, 2) VoLTE, 3) WhatsApp video call, 4) data uploading through file transfer protocol (FTP), and 5) FTP data downloading.

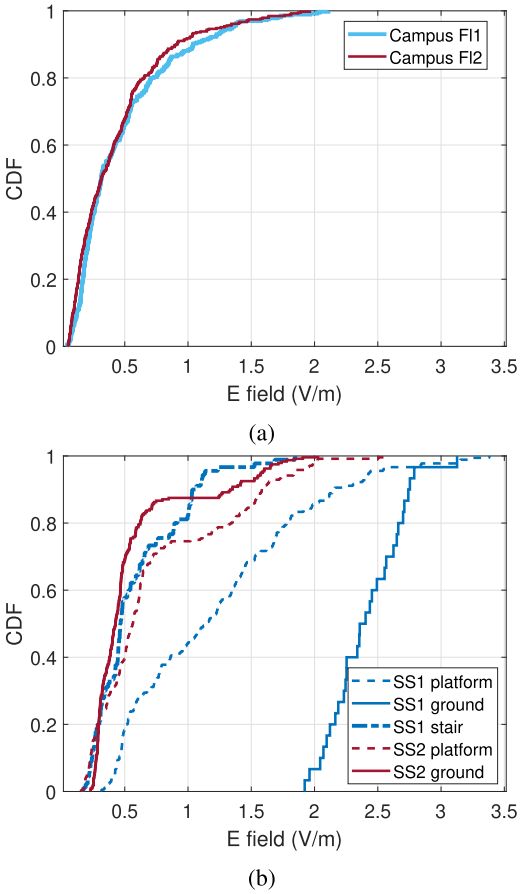

FIGURE 4. Statistical distribution of the total E-field (V/m) for 'DAS on' scenario: (a) the campus, (b) SS1 and SS2.

For circuit voice calls (occurring over 3G connections) and VoLTE calls (occurring over 4G connections), each voice call lasts 2 min. We note that the experimenter was holding the Nemo Handy close to his ear and established a conversation with another remote person in order to emulate a normal traffic. We also utilized the same settings for the WhatsApp video call (occurring over either 3G or 4G connections), with a difference that the mobile phone was held in front of the person. For data uploading to an FTP server, 100 MB file size (UL100) was used for 'DAS off' scenario or over 3G connections. In contrast, for 'DAS on' scenario over 4G connections, both 100 MB and 500 MB file sizes (UL500) were used alternatively. Also, a 500 MB file (DL500) was downloaded over 4G connections. For data downloading and uploading, the mobile phone was held in front of the person.

IV. RESULTS

A. ANALYSIS OF DL EXPOSURE

The DL exposure induced by base stations and/or DAS antennas was measured covering the area on the campus and two underground subway stations for both 'DAS on' and 'DAS off' scenarios. The results are reported in Table 2, where for each measurement point, the total E-field is averaged over 30 repetitions. Then, for each floor, an average

TABLE 2. Average total E-field (V/m) for each measurement point in different locations. (NF = Noise Floor).

DAS	Location	Measurement points												Mean	std deviation
		P1	P2	P3	P4	P5	P6	P7	P8	P9	P10	P11	P12		
ON	SS1 Platform	1.39	2.03	1.2	0.86	0.47	0.42	-	-	-	-	-	-	1.2	0.7
	SS1 Stair	0.25	0.86	0.44	-	-	-	-	-	-	-	-	-	0.57	0.35
	SS1 Ground	2.14	-	-	-	-	-	-	-	-	-	-	-	2.14	0.29
	SS2 Platform	1.2	1.58	0.54	0.62	0.5	0.38	0.24	0.19	-	-	-	-	0.8	0.53
	SS2 Ground	1.35	0.3	0.38	0.27	0.46	0.45	0.61	0.29	-	-	-	-	0.61	0.4
	Campus Fl1	0.62	1.12	0.65	0.55	0.27	0.29	0.32	0.64	1.01	0.97	0.32	0.20	0.66	0.37
	Campus Fl2	1.03	0.56	0.77	0.54	0.51	0.25	0.34	0.32	0.28	0.84	0.25	0.22	0.56	0.37
OFF	SS1 Platform	NF	NF	NF	NF	NF	NF	-	-	-	-	-	-	NF	-
	SS1 Stair	NF	NF	NF	-	-	-	-	-	-	-	-	-	NF	-
	SS1 Ground	0.48	-	-	-	-	-	-	-	-	-	-	-	0.48	0.31
	SS2 Platform	NF	NF	NF	NF	-	-	-	-	-	-	-	-	NF	-
	SS2 Ground	0.25	-	0.28	-	-	-	0.35	0.23	-	-	-	-	0.28	0.2
	Campus Fl1	NF	NF	NF	NF	NF	NF	NF	NF	NF	NF	NF	NF	NF	-
	Campus Fl2	NF	NF	NF	NF	NF	NF	NF	NF	NF	NF	NF	NF	NF	-

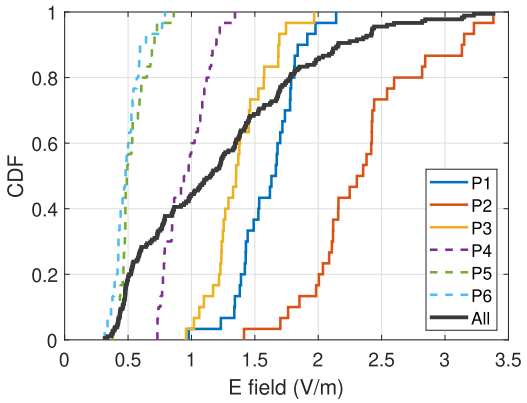

FIGURE 5. Statistical distribution of the total E-field at SS1 platform for 'DAS on' scenario across different measurement points.

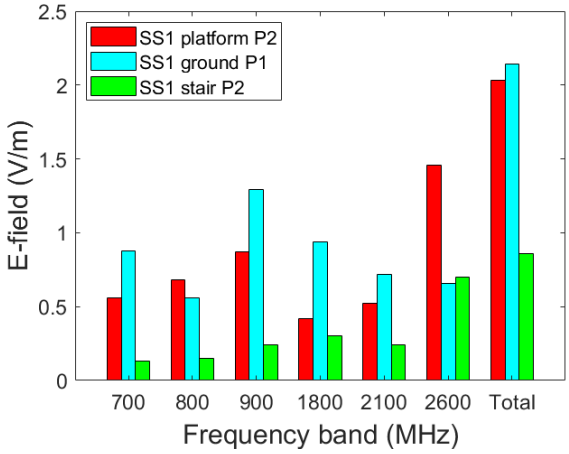

FIGURE 6. Average E-field per frequency band and average total E-field across different floors of SS1 for 'DAS on' scenario.

E-field and a standard (std) deviation are computed after aggregating all the 30 repetitions of all the measurement points, whose cumulative distribution functions (CDF) are displayed in Fig. 4 for 'DAS on' scenario. Starting with 'DAS off' scenario, we notice that the E-field strength values at most selected indoor places are less than the noise floor (NF) of the equipment, which is equal to 0.04 V/m. This means that these values are very low. The exception occurs for the ground levels of both subway stations, where the E-field strength presents non negligible values above the NF, varying between 0.23 V/m and 0.48 V/m. These results confirm our observations related to cartoradio (in Section III-A), where nearby outdoor base stations allow radio covering of the ground levels of both subway stations but are not able to reach the underground levels. For the campus, outdoor base stations are relatively far away.

For 'DAS on' scenario, the average total E-field strength values change between 0.25 V/m and 2.14 V/m for SS1, while they are between 0.19 V/m and 1.58 V/m for SS2. For both floors of the campus, these values change between 0.2 V/m and 1.12 V/m. Obviously, turning on the DAS slightly increases the DL E-field levels. The statistical distribution of the total E-field strength at each measurement point on the SS1 platform is shown in Fig. 5. According to the floorplan in Fig. 2c, the point P2 corresponds to the maximum E-field point where the E-field reaches the maximum value. The distances to the DAS antenna are increasing from points P3 to P6, implying a decrease on the E-field strength. Even though P1 is the closest point to the DAS antenna, the E-field is not the highest because it is not located in the main direction of the antenna. Similar results are seen for SS2 platform.

Furthermore, we show in Fig. 6 the variation of the E-field values over the cellular frequency bands for three selected points on different floor levels of SS1. Each selected point corresponds to the maximum E-field value. The results show that the decomposition of the E-field over the frequency bands differs with the location as well as with the radio technology. Most DL exposure is due to the 2600 MHz LTE frequency band for both SS1 platform and stair, and the 900 MHz UMTS/GSM frequency band for SS1 ground level. Table 3 shows the E-field values per frequency band, averaged over all the measurement points of each floor. We note that in the campus, just two technologies are available: i.e., 4G over 2600 MHz and 3G over 2100 MHz, where 70% of the DL exposure is due to the 2600 MHz

TABLE 3. Average E-field per frequency band in different locations for 'DAS on' scenario.

	Mean E (V/m)						Percentage limit (%)					
Location	700	800	900	1800	2100	2600	700	800	900	1800	2100	2600
SS1 Platform	0.36	0.42	0.44	0.36	0.43	0.76	1	1.08	1.07	0.62	0.7	1.25
SS1 Stair	0.12	0.11	0.22	0.22	0.15	0.42	0.33	0.29	0.55	0.38	0.25	0.7
SS1 Ground	0.88	0.56	1.29	0.94	0.72	0.66	2.44	1.44	3.15	1.62	1.18	1.08
SS2 Platform	0.22	0.27	0.48	0.21	0.33	0.36	0.61	0.69	1.17	0.36	0.54	0.59
SS2 Ground	0.22	0.27	0.3	0.17	0.24	0.28	0.62	0.7	0.72	0.29	0.39	0.45
Campus Fl1	-	-	-	-	0.21	0.62	-	-	-	-	0.34	1.02
Campus Fl2	-	-	-	-	0.24	0.5	-	-	-	-	0.39	0.82

frequency band. Moreover, Table 3 shows the percentage ratio of the E-field to the corresponding ICNIRP limits [7], with a maximum value of 3.15%. This means that even though deploying indoor DAS antennas increases the E-field values (or alternatively the DL exposure), these values remain very far below the standard limits.

B. ANALYSIS OF UL EXPOSURE

Unlike the DL exposure, the UL exposure is sporadic and relies on the mobile phone usage. Accordingly and given that Nemo Handy allows recording values every 1 second, the number of samples per usage service can not be constant. For instance, it is inversely proportional to the throughput for data uploading/downloading while considering the size of the transferred file. Moreover, the statistics are constructed over the available frequency bands and up to two network operators. While only two frequency bands of a single operator are available at the campus, the frequency bands ranging from 700 MHz to 2600 MHz are available on the subway stations. Due to some measurement constraints, particularly for the subway stations, the UL measurements using the Nemo Handy were not performed at all the planned measurement points for each floor. However, they were conducted at one or two points on each floor, including the point of maximum E-field. Furthermore, we note that the statistics size differs according to the active state of the DAS antennas. For 'DAS off' scenario, the cellular connection may fail to be established and the usage service may experience a poor quality and take a very long time.

Starting with the measurements performed at the campus for data uploading (UL100) over 4G connections, the results of both mobile TX power and throughput at different measurement points on both floors and for both 'DAS on' and 'DAS off' scenarios are shown in Fig. 7. With the DAS turned off, the results show that the mobile phone emits very high powers (almost equal or close to the maximum 23 dBm) with low achievable throughput (changing from almost 0 up to 10 Mbps). With turning on the DAS, we can easily notice an opposite behavior where the TX powers explicitly decrease (with values changing between -18 and 15 dBm) and the throughput strongly increases (with values changing between 20 and 32 Mbps). We note that the variation over the different measurement points is more random than in the case of DL since the UL TX power relies on multiple parameters including the relative distance to the DAS antenna, the traffic load, the shadowing (e.g., how we held the mobile phone), the usage service, and the allocated resource blocks.

For each location and mobile usage service, TX powers and throughput are averaged over the measurement points, the frequency bands, and the network operators. The results are summarized in Table 4 for both 4G and 3G connections. Starting with data uploading over 4G connections, for respectively SS1 platform, SS1 stair, and SS1 ground, the TX powers are 18.5, 22.1, and 19.1 dBm for 'DAS off' scenario, while they are 8.4, 9.2, and 4 dBm for 'DAS on' scenario; the throughput are 43.7, 1.7, and 14.2 Mbps for 'DAS off', while they are 40.8, 35.3, and 34.4 Mbps for 'DAS on'. From 'DAS off' to 'DAS on' scenarios, TX powers are reduced by factors of about 10, 13, and 15 dB for respectively platform, stair, and ground. An important increase on the throughput is shown for the stair with a factor of about 21. Much lower factor is shown for the ground, with a value of around 2. However, the throughput on the platform remains almost the same for 'DAS on' and 'DAS off' scenarios. Similarly for SS2, turning on DAS antennas decreases the TX powers with approximately 9 dB and increases the throughput with factors of 5.6 for SS2 platform and 2.2 for SS2 ground. Indeed for respectively SS2 platform and SS2 ground, the TX powers are about 21.9 and 18.7 dBm for 'DAS off', while they are about 12.3 and 9.4 dBm for 'DAS on' scenario; the throughput are about 6.1 and 16.1 Mbps for 'DAS off' while the values are about 33.9 and 34.8 Mbps for 'DAS on'.

At the platform and the ground level of the subway stations for 'DAS off' scenario, the TX powers are almost 4 dB lower than the UE maximum output power, i.e., 23 dBm. Moreover, the throughput is very high, even very close to that of 'DAS on' scenario. These results at the ground level and the platform are respectively explained by the alternative or additional coverage ensured by outdoor base stations and DAS antennas of the subway station's tunnel, which remain enabled all the time. More specifically, we note that the throughput at SS1 platform is slightly higher in the case of 'DAS off' than in the case of 'DAS on'. In addition to the previous reason, we note that the average throughput for 'DAS on' scenario is decreased due to connections over the 800 MHz frequency band, which does not exist for 'DAS off' scenario. Indeed for 'DAS on' scenario, the throughput at 800 MHz is almost the half of that provided by 2600 and 1800 MHz.

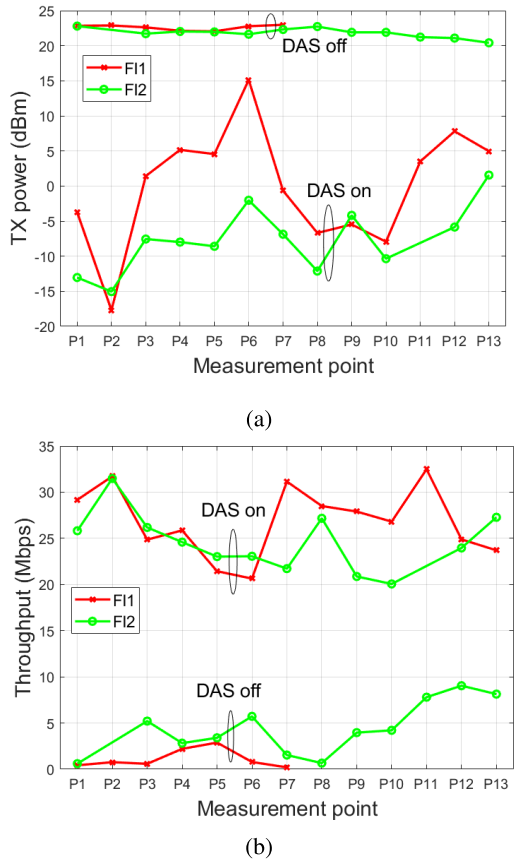

FIGURE 7. Variation of both (a) average TX power and (b) average throughput across the measurement points, when considering UL100 over 4G connections at the campus.

Almost similar trends are seen for the remaining mobile usages for both 4G and 3G connections. Furthermore, we note that the connection in most 'DAS off' scenarios was very poor since it was difficult to establish a voice call, which did not connect easily most times or dropped quickly. For the video calls, the video quality was very poor and distorted. This reveals that deploying indoor DAS antennas can decrease the average TX powers and increase the average throughput, resulting in less UL exposure as well as better connection quality.

C. IMPACT OF DAS ON THE GLOBAL EXPOSURE

As explained previously, EI allows assessing the global exposure taking into account simultaneously the UL and the DL. According to equation 1, we compute average partial EI values per floor for each given location and for 'DAS on' and 'DAS off' scenarios. We calculate the EI for an UL operating specifically on the 2600 MHz frequency band, while the DL covers all available frequency bands. Moreover, we take into account the position of the individual, such as a sitting person at the campus or a standing person in the subway station, and subsequently choose the appropriate reference WBSAR value (from Table 1) based on the type of usage service being used (i.e., voice or data). In particular, we select the

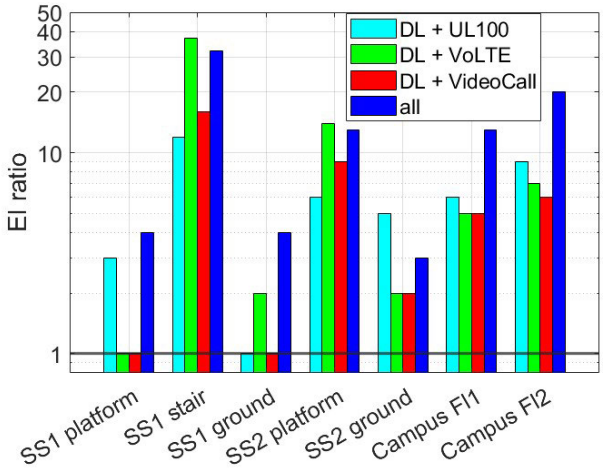

FIGURE 8. EI ratios of 'DAS off' to 'DAS on'.

WBSAR corresponding to data for both video calls and data uploading since the mobile phone is assumed in front of the human body. As the average EI is computed per floor, the average incident power densities per frequency band ($\bar{S}_f^{inc}$) and average mobile emitted powers ($\bar{P}_{f,u}^{TX}$) are obtained from Table 3 and Table 4, respectively. In order to emphasize the impact of deploying indoor DAS antennas on the global EMF exposure, we evaluate the ratio of the EI in 'DAS off' scenario to the EI in 'DAS on' scenario, i.e., EI ratio=EI (DAS off) / EI (DAS on).

In a typical subway station, a passenger spends around few minutes at the platform while waiting to take the train. This duration could change on average from few seconds up to 7 min (1 train every 3 to 7 min). Therefore, we consider a total exposure time duration of $T = 7$ min for the subway station case, regardless at which floor the person is. Given that the campus is a working place, we consider an exposure time duration of $T = 8$ hours, corresponding to the average working hours per day in France. The UL exposure duration depends on each usage service u. We consider, respectively for the subway station and the campus, 2 min and 30 min for the data uploading; 2 min and 10 min for the VoLTE/video call. For the UL part, we evaluate EI for several combinations of usage services, i.e., DL + UL100, DL + VoLTE, DL + video call, and all (DL + UL100 + VoLTE + video call), which allows accounting for different types of user profiles.

The results of the EI ratios between 'DAS off' and 'DAS on' are presented in Fig. 8. These ratios differ from one location to another. EI ratios higher than 5 are seen for SS1 stair, SS2 platform, and both floors of the campus, where there is no radio coverage when DAS is turned off. With turning on the DAS antennas, the global exposure EI is decreased with at least a factor of 5. This means that, for 'DAS on', the decrease in the UL exposure is much more important than the increase in the DL exposure. On the other hand, small EI ratios (between 1 and 4) are seen for the remaining

TABLE 4. Synthesis of UL exposure parameters (TX power and throughput) for both 4G and 3G connections.

DAS	Location	TX power (dBm)						Throughput (Mbps)		
		4G			3G			4G		3G
		UL100 (500)	VoLTE	VideoCall	UL100	VoiceCall	VideoCall	UL100 (500)	DL500	UL100
ON	SS1 Platform	8.4	0.1	2.2	-42.5	-26.3	-35.9	40.8	104.5	2.9
	SS1 Stair	9.2	3.4	2.4	-29.3	-20.3	-23.4	35.3	126.5	2.7
	SS1 Ground	4	-6	-1.1	-35.7	-27.1	-33.1	34.4	133.3	2.6
	SS2 Platform	12.3	7.6	8.1	-22.7	-14.4	-16.4	33.9	105	3
	SS2 Ground	9.4	10.3	12.4	-19.3	-4.3	-18.8	34.8	-	2.3
	Campus Fl1	6.1 (7.1)	-5.7	6.7	-38.1	-25.1	-40	26.9 (27.7)	85.1	3.7
	Campus Fl2	-5.1 (-1.8)	-7.1	5.5	-45.3	-33.7	-41.8	24.6 (26.4)	77.4	4.1
OFF	SS1 Platform	18.5	12.5	14.4	6.1	-6	7.1	43.7	49.4	1.3
	SS1 Stair	22.1	22.5	20.2	20.4	2.3	19.8	1.7	-	0.2
	SS1 Ground	19.1	18.9	18.4	-3.2	-8.4	-3.7	14.2	16.6	2.1
	SS2 Platform	21.9	21.8	21.7	21.1	18.4	18.9	6.1	2.2	0.5
	SS2 Ground	18.7	15.1	16.1	-20.3	-17.6	-14.9	16.1	-	2.4
	Campus Fl1	22.6	23	23	18.2	-	-	1.1	-	0.4
	Campus Fl2	21.9 (22.6)	23	23	19.8	-	-	4.4 (0.7)	-	0.5

locations, i.e., SS1 platform, SS1 ground, and SS2 ground. While SS1 ground and SS2 ground are covered with outdoor base stations, SS1 platform is covered with DAS antennas of the tunnel. This implies that the relative decrease in the UL exposure with respect to the increase in the DL exposure with turning off the DAS is less significant than the previous case. Furthermore, for each location, the EI ratio changes according to the usage service. This depends on how the person is handling his mobile phone (e.g., on the head or in front of the human body). It is also related to how much the DAS antennas will decrease on average the UL exposure with respect to the DL. It is noteworthy that the EI ratios given in Fig. 8 are average values and might change with the user profile, depending on which usage services he is using and for how long duration.

V. DISCUSSION

We carried out measurement campaigns in two subway stations and an organization's building, where we had the capability to selectively turn off specific DAS antennas. This enabled us to assess the contribution of these DAS antennas to the overall EMF exposure. Our study revealed that the deployment of indoor DAS systems leads to a slight increase in the radiated E-field (DL exposure), accompanied by a heavily reduced output power of mobile phones and improved overall throughput. As a result, there was an average decrease in the global EMF exposure as measured by EI. These trends were consistent with observations made when comparing the behavior of femto or small cell networks to macro cell networks in various settings and environments [15], [16], [18].

The exposure index EI was computed using specific assumptions on time usage, which are based on the characteristics and nature of the selected environment. The EI was also analyzed for various combinations of usage services. Overall, while these assumptions may not be accurate for every individual, they provide a useful framework for understanding and analyzing behavioral trends for various types of users. To further enhance the analysis, it would be beneficial to consider different types of user profiles in diverse scenarios, as addressed in [40], and [41].

On the other hand, the results highlighted that the extent of global exposure reduction in a given area is heavily influenced by the presence of additional RF coverage. Significant reductions in EI were observed in scenarios where there was minimal additional RF coverage, such as the campus and the stair in SS1. These findings emphasize the need for proactive and optimized planning strategies for DAS deployment to effectively manage both network performance and EMF exposure, particularly in environments with varying levels of RF coverage. While the presented results provide insights into various configurations and scenarios, it is important to note that the degree of global exposure reduction may vary depending on several factors as discussed previously. Nevertheless, these findings can be extrapolated and generalized to similar environments, serving as a basis for understanding and addressing EMF exposure concerns while considering the specific aspects and requirements of each setting.

The EI was computed using the whole body SAR, which is appropriate for evaluating the overall impact of DAS on the average EMF exposure of a population in a given area. This approach is justified since the UL exposure in this study considers various phone usages that may affect the SAR distribution across different organs of the body. For instance, during voice calls, when the mobile phone is held against the ear, the exposure is concentrated in the brain [25]. Conversely, during data uploading/downloading and WhatsApp video calls, the mobile phone is typically held in front of the body. However, it is important to acknowledge the uncertainty in our assumptions, as users may utilize alternative methods such as speaker mode or earphones, which could alter the specific exposure patterns. Furthermore, additional uncertainties can arise from factors such as the mobile phone model, including the location of the transmitter antenna, antenna switching capabilities, time average SAR (TAS), and other related parameters. These factors can introduce variability in the actual SAR

distribution. Nevertheless, despite these uncertainties, the use of whole body SAR provides a practical and reasonable means to assess the average EMF exposure in the context of our study.

VI. CONCLUSION

The objective of the present work is to assess the contribution of distributed antenna systems on the global human exposure. This is achieved by conducting a measurement campaign in an organization's building (known as the campus) and two subway stations, with the capability to turn on and off the DAS antennas. With turning on the DAS antennas, the E-field strength slightly increases with highest values shown in the immediate vicinity of DAS antennas, either under the omnidirectional antenna or in front of the directive antenna. However, these values are very far below the ICNIRP limits, with a maximum percentage limit of 3.15%. Furthermore, the results showed that deploying an indoor DAS improves the radio coverage, in terms of throughput, while significantly decreases the power emitted by the mobile phone. This implies a significant decrease in the UL exposure. Considering both UL and DL, the average global exposure, quantified with the exposure index EI, is reduced with activating the DAS antennas. The reduction factors depend on the usage service, the posture, and the user profile. Moreover, these factors depend on whether additional distant RF sources are present. For instance, very high reduction factors are shown for location where there is no additional RF coverage.

ACKNOWLEDGMENT

The authors thank Rennes Métropole and Keolis Rennes for allowing them to carry out the measurements in the subway stations. They also thank TDF for allowing access to its premises. They particularly thank Allal OUBEREHIL for his support and the TDF transmission support team for their availability to carry out DAS "switch on/switch off" operations.

REFERENCES

[1] (May 2018). *L'excés de temps passé À L'intérieur: Un Enjeu De Santé Pour la Génération 'Indoor'*. VELUX. [Online]. Available: https://presse.velux.fr/generation-indoor/

[2] L. M. Correia, *Wireless Flexible Personalised Communications*. Hoboken, NJ, USA: Wiley, 2001.

[3] E. Bernardi, S. Carlucci, C. Cornaro, and R. Bohne, "An analysis of the most adopted rating systems for assessing the environmental impact of buildings," *Sustainability*, vol. 9, no. 7, p. 1226, Jul. 2017.

[4] C. de la O Millán, T. B. Sørensen, and N. M. Mikkelsen, "A study on the radio coverage in underground stations of the new Copenhagen metro system," in *Proc. 8th ACM Workshop Perform. Monitor. Meas. Heterogeneous Wireless Wired Netw.*, Nov. 2013, pp. 99–106.

[5] A. A. M. Saleh, A. Rustako, and R. Roman, "Distributed antennas for indoor radio communications," *IEEE Trans. Commun.*, vol. COM-35, no. 12, pp. 1245–1251, Dec. 1987.

[6] R. Heath, S. Peters, Y. Wang, and J. Zhang, "A current perspective on distributed antenna systems for the downlink of cellular systems," *IEEE Commun. Mag.*, vol. 51, no. 4, pp. 161–167, Apr. 2013.

[7] International Commission on Non-Ionizing Radiation Protection, "Guidelines for limiting exposure to electromagnetic fields (100 kHz to 300 GHz)," *Health Phys.*, vol. 118, no. 5, pp. 483–524, May 2020.

[8] J. Wiart, *Radio-Frequency Human Exposure Assessment: From Deterministic to Stochastic Methods*. Hoboken, NJ, USA: Wiley, 2016.

[9] *Evolved Universal Terrestrial Radio Access (E-UTRA); Physical Layer Procedures*, document TS 36.213, 3GPP, 2009.

[10] A. Gati, E. Conil, M.-F. Wong, and J. Wiart, "Duality between uplink local and downlink whole-body exposures in operating networks," *IEEE Trans. Electromagn. Compat.*, vol. 52, no. 4, pp. 829–836, Nov. 2010.

[11] *EU FP7 LEXNET (Low EMF Exposure Future Networks) Project*. Accessed: Dec. 11, 2022. [Online]. Available: http://www.lexnet-project.eu/ and https://cordis.europa.eu/project/id/318273

[12] M. Tesanovic, E. Conil, A. De Domenico, R. Aguero, F. Freudenstein, L. M. Correia, S. Bories, L. Martens, P. M. Wiedemann, and J. Wiart, "The LEXNET project: Wireless networks and EMF: Paving the way for low-EMF networks of the future," *IEEE Veh. Technol. Mag.*, vol. 9, no. 2, pp. 20–28, Jun. 2014.

[13] E. Chiaramello, M. Bonato, S. Fiocchi, G. Tognola, M. Parazzini, P. Ravazzani, and J. Wiart, "Radio frequency electromagnetic fields exposure assessment in indoor environments: A review," *Int. J. Environ. Res. Public Health*, vol. 16, no. 6, pp. 1–29, 2019.

[14] A. Boursianis, P. Vanias, and T. Samaras, "Measurements for assessing the exposure from 3G femtocells," *Radiat. Protection Dosimetry*, vol. 150, no. 2, pp. 158–167, Jun. 2012.

[15] S. Aerts, D. Plets, L. Verloock, L. Martens, and W. Joseph, "Assessment and comparison of total RF-EMF exposure in femtocell and macrocell base station scenarios," *Radiat. Protection Dosimetry*, vol. 162, no. 3, pp. 236–243, Dec. 2014.

[16] S. Aerts, D. Plets, A. Thielens, L. Martens, and W. Joseph, "Impact of a small cell on the RF-EMF exposure in a train," *Int. J. Environ. Res. Public Health*, vol. 12, no. 3, pp. 2639–2652, Feb. 2015.

[17] T. Mazloum, B. Fetouri, N. Elia, E. Conil, C. Grangeat, and J. Wiart, "Assessment of RF human exposure to LTE small-and macro-cells: UL case," in *Proc. 11th Eur. Conf. Antennas Propag. (EUCAP)*, Mar. 2017, pp. 1592–1593.

[18] T. Mazloum, S. Aerts, W. Joseph, and J. Wiart, "RF-EMF exposure induced by mobile phones operating in LTE small cells in two different urban cities," *Ann. Telecommun.*, vol. 74, nos. 1–2, pp. 35–42, Feb. 2019.

[19] T. Kopacz, C. BornKessel, M. Hein, and D. Heberling, "Investigation of LTE user equipment transmit power control and comparison of uplink exposure between small and macro cell environment," in *Proc. BioEM*, 2017, pp. 1–2.

[20] *Rapport Technique Sur Les Déploiements Pilotes Des Petites Antennes en France*, ANFR, Maisons-Alfort, France, 2018.

[21] S. Wang and J. Wiart, "Sensor-aided EMF exposure assessments in an urban environment using artificial neural networks," *Int. J. Environ. Res. Public Health*, vol. 17, no. 9, pp. 60–70, Apr. 2020.

[22] T. Mazloum, S. Wang, M. Hamdi, B. A. Mulugeta, and J. Wiart, "Artificial neural network-based uplink power prediction from multi-floor indoor measurement campaigns in 4G networks," *Front. Public Health*, vol. 9, Nov. 2021, Art. no. 777798.

[23] S. Wang, T. Mazloum, and J. Wiart, "Prediction of RF-EMF exposure by outdoor drive test measurements," *Telecom*, vol. 3, no. 3, pp. 396–406, Jun. 2022.

[24] M. Mallik, S. Kharbech, T. Mazloum, S. Wang, J. Wiart, D. P. Gaillot, and L. Clavier, "EME-Net: A U-net-based indoor EMF exposure map reconstruction method," in *Proc. 16th Eur. Conf. Antennas Propag. (EuCAP)*, Mar. 2022, pp. 1–5.

[25] A.-K. Lee and H.-D. Choi, "Brain EM exposure for voice calls of mobile phones in wireless communication environment of Seoul, Korea," *IEEE Access*, vol. 8, pp. 163176–163185, 2020.

[26] P. Joshi, D. Colombi, B. Thors, L. Larsson, and C. Törnevik, "Output power levels of 4G user equipment and implications on realistic RF EMF exposure assessments," *IEEE Access*, vol. 5, pp. 4545–4550, 2017.

[27] M. Celaya-Echarri, L. Azpilicueta, V. Ramos, P. Lopez-Iturri, and F. Falcone, "Empirical and modeling approach for environmental indoor RF-EMF assessment in complex high-node density scenarios: Public shopping malls case study," *IEEE Access*, vol. 9, pp. 46755–46775, 2021.

[28] P. Joshi, F. Ghasemifard, D. Colombi, and C. Törnevik, "Actual output power levels of user equipment in 5G commercial networks and implications on realistic RF EMF exposure assessment," *IEEE Access*, vol. 8, pp. 204068–204075, 2020.

[29] C. Törnevik, T. Wigren, S. Guo, and K. Huisman, "Time averaged power control of a 4G or a 5G radio base station for RF EMF compliance," *IEEE Access*, vol. 8, pp. 211937–211950, 2020.

[30] Azenqos. Accessed: Dec. 9, 2022. [Online]. Available: https://www2.azenqos.com/
[31] Rohde & Schwarz. *QualiPoc Android*. Accessed: Dec. 11, 2022. [Online]. Available: https://www.rohde-schwarz.com/us/products/test-and-measurement/network-data-collection/qualipoc-android_63493-55430.html
[32] Keysight. *Nemo Handy*. Accessed: Dec. 11, 2022. [Online]. Available: https://www.keysight.com/fr/en/product/NTH00000B/nemo-handy-handheld-measurement-solution.html
[33] T. Mazloum, AMN. Danjou, J. Schûz, S. Bories, A. Huss, E. Conil, I. Deltour, and J. Wiart, "XMobiSensePlus: An updated application for the assessment of human exposure to RF-EMFs," in *Proc. 33rd Gen. Assem. Scientific Symp. Int. Union Radio Sci.*, Aug. 2020, pp. 1–2.
[34] S. Bories, "Personal exposimeter to monitor EMF up-link exposure from daily-usages of mobile phone," in *Proc. BioEM*, 2018, pp. 1–4.
[35] S. Aerts, J. Wiart, L. Martens, and W. Joseph, "Long-term spatio-temporal RF-EMF exposure assessment in a sensor network," in *Proc. Joint Annu. Meeting Bioelectromagn. Soc. Eur. BioElectromagn. Assoc. (BioEM)*, pp. 279–283, 2018.
[36] S. Iakovidis, C. Apostolidis, A. Manassas, and T. Samaras, "Electromagnetic fields exposure assessment in Europe utilizing publicly available data," *Sensors*, vol. 22, no. 21, p. 8481, Nov. 2022.
[37] C. R. Bhatt, M. Redmayne, M. J. Abramson, and G. Benke, "Instruments to assess and measure personal and environmental radiofrequency-electromagnetic field exposures," *Australas. Phys. Eng. Sci. Med.*, vol. 39, no. 1, pp. 29–42, Mar. 2016.
[38] C. R. Bhatt, S. Henderson, C. Brzozek, and G. Benke, "Instruments to measure environmental and personal radiofrequency-electromagnetic field exposures: An update," *Phys. Eng. Sci. Med.*, vol. 45, pp. 687–704, Jun. 2022.
[39] N. Varsier, Y. Huang, A. Krayni, A. Hadjem, J. Wiart, G. Vermeeren, D. Plets, W. Joseph, L. Martens, C. Oliveira, D. Sebastião, M. Ferreira, F. Cardoso, L. Correia, M. Koprivica, M. Popovic, E. Kocan, and M. Pejanovic-Djurisic, *LEXNET Low EMF Exposure Future Networks: Deliverable D2.8 Global Wireless Exposure Metric Definition*, LEXNET Consortium, Moulineaux, France, document D2.8, 2015.
[40] N. Varsier, D. Plets, Y. Corre, G. Vermeeren, W. Joseph, S. Aerts, L. Martens, and J. Wiart, "A novel method to assess human population exposure induced by a wireless cellular network," *Bioelectromagnetics*, vol. 36, no. 6, pp. 451–463, Sep. 2015.
[41] Y. Huang and J. Wiart, "Simplified assessment method for population RF exposure induced by a 4G network," *IEEE J. Electromagn., RF Microw. Med. Biol.*, vol. 1, no. 1, pp. 34–40, Jun. 2017.
[42] C. Oliveira, M. Mackowiak, and L. M. Correia, "Exposure assessment of smartphones and tablets," in *Proc. Int. Symp. Wireless Commun. Syst. (ISWCS)*, Aug. 2015, pp. 436–440.
[43] E. Conil, A. Hadjem, F. Lacroux, M. F. Wong, and J. Wiart, "Variability analysis of SAR from 20 MHz to 2.4 GHz for different adult and child models using finite-difference time-domain," *Phys. Med. Biol.*, vol. 53, no. 6, pp. 1511–1525, Feb. 2008.
[44] A. Christ, W. Kainz, E. G. Hahn, K. Honegger, M. Zefferer, E. Neufeld, W. Rascher, R. Janka, W. Bautz, J. Chen, B. Kiefer, P. Schmitt, H.-P. Hollenbach, J. Shen, M. Oberle, D. Szczerba, A. Kam, J. W. Guag, and N. Kuster, "The Virtual Family—Development of surface-based anatomical models of two adults and two children for dosimetric simulations," *Phys. Med. Biol.*, vol. 55, no. 2, pp. N23–N38, Dec. 2009.
[45] Cartoradio of the Agence Nationale des Fréquences Radio (ANFR). *La Carte des Sites et des Mesures Radioélectriques*. Accessed: Nov. 4, 2021. [Online]. Available: https://www.cartoradio.fr
[46] *ANFR-Protocole de Mesure*. Accessed: Dec. 11, 2022. [Online]. Available: https://www.anfr.fr/fileadmin/mediatheque/documents/expace/Protocole-mesure-15-4.1.pdf

TAGHRID MAZLOUM (Member, IEEE) received the M.E. degree in electronics and telecommunication engineering and the M.S. degree in telecommunication systems from Lebanese University, Tripoli, Lebanon, in 2012, and the Ph.D. degree in electronics and communications from Télécom Paris, Paris, France, in 2016.

She is currently a Research Engineer with CEA-Leti, Grenoble, France. Previously, she was a Research Engineer with the Chaire C2M "Caractérisation, modélisation et maitrise," Télécom Paris, Institut Mines Telecom, Paris. Her research interests include radio propagation, channel modeling, EMF exposure, EMF dosimetry, reconfigurable intelligent surface (RIS)-assisted wireless communication channel, machine learning for applications in wireless communications, and physical layer security.

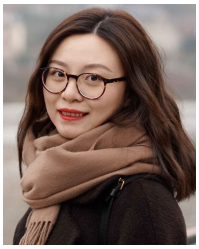

SHANSHAN WANG (Member, IEEE) was born in Nanjing, China, in 1991. She received the B.Sc. degree in communications engineering from Soochow University, Suzhou, China, in 2013, the M.Sc. degree (Hons.) in wireless communication and signal processing from the University of Bristol, Bristol, U.K., in 2014, and the Ph.D. degree from the Laboratory of Signals and Systems, Paris-Saclay University, Paris, France, in 2019. From 2015 to 2018, she was with the French National Center for Scientific Research (CNRS), Paris, as an Early Stage Researcher of the European-Funded Project H2020 ETN-5Gwireless. She is currently a Postdoctoral Researcher with Télécom Paris, IP Paris, France. Her research interests include stochastic geometry, EMF exposure, and machine learning for applications in wireless communications. She was a recipient of the 2018 INISCOM Best Paper Award. She served as the Guest Editor for the MDPI *Sensors*, in 2022.

JOE WIART (Senior Member, IEEE) received the Diploma degree in telecommunication engineering in 1992, the Ph.D. degree in 1995, and the H.D.R. degree in 2015. Since 2015, he has been the holder of the Chaire C2M "Caractérisation, modélisation et maitrise," Télécom Paris, Institut Mines Telecom. His works gave rise to more than 170 publications in journal articles and more than 200 communications. His research interests include experimental, numerical methods, machine learning, and statistics applied in electromagnetism and dosimetry. He is the Chairperson of the TC106x of the European Committee for Electrotechnical Standardization (CENELEC), in charge of EMF exposure standards. He was the Chairperson of the International Union of Radio Science (URSI) Commission k, from 2014 to 2021, and the French Chapter of URSI, from 2009 to 2012. He has been an Emeritus Member of the Society of Electrical Engineers (SEE), since 2008.